Astron. Astrophys. 234, 299–307 (1990)

ASTRONOMY AND ASTROPHYSICS

Optical spectra of ζ Aurigae binary systems

II. The lower chromosphere of ζ Aurigae

K.-P. Schröder[1,⋆], R.E.M. Griffin[2,⋆], and R.F. Griffin[2,⋆]

[1] Hamburger Sternwarte, Gojenbergsweg 112, D-2050 Hamburg 80, Federal Republic of Germany
[2] Institute of Astronomy, The Observatories, Madingley Road, Cambridge CB3 0HA, England

Received July 31, accepted November 24, 1989

Abstract. High-resolution spectra of the 1987 eclipse of ζ Aur at chromospheric and partial phases (during ingress) yield height resolution and enable us to model empirically the lower chromospheric layers of the K-supergiant primary star. We apply curves of growth to analyze chromospheric absorption spectra, and take into account the fact that the B star has an appreciable disk. The final column densities are modelled numerically by a simple density/height relationship for each observed atomic species, and yield ionization ratios Fe II: Fe I and Mg II: Mg I. By comparing the ionization equilibria of iron and magnesium we can calculate the following electron densities: at a height of $2.3\,10^6$ km above the stellar limb, $\log n_e = 9.6 \pm 0.3$, or 1.8% ionization of hydrogen; at $6.1\,10^6$ km, $\log n_e = 9.2 \pm 0.2$ or about 5% ionization of hydrogen. We also estimate the electron temperature T_e to be approximately 5500 K at both heights.

Key words: stars: atmospheres of – stars: chromospheres of – stars: individual – stars: binaries: spectroscopic – stars: supergiant

1. Introduction

Analysis of the eclipses of ζ Aur systems has a long history. A classical ζ Aur binary is comprised of a K supergiant and a B dwarf in a detached eclipsing system. Near to its occultation, the B dwarf shines through chromospheric material of the K star and thereby constitutes a probing light source; the movement of the line of sight with orbital motion provides height resolution of the K-star chromosphere, and thus furnishes the only possibility of obtaining height-resolved information about a stellar chromosphere except in the case of the Sun. During the so-called atmospheric-eclipse stage the B-star spectrum contains additional phase-dependent chromospheric absorption lines. Unfortunately, the complex K-star spectrum, which itself includes lines corresponding to the chromospheric ones, unavoidably contributes to the observed spectrum of the system, which cannot be resolved on the slit of the spectrograph. The observed composite spectrum therefore has three components superimposed, and careful isolating procedures are required in order to disentangle the separate contributions. In the classical photographic region the K-star flux contributes typically between 40% and 80% of the total flux, and early optical investigations of ζ Aur chromospheric-eclipse spectra (e.g. Wilson, 1960, and references therein) were severely circumscribed by problems of contamination by the K-star spectrum. Limitations to the interpretations of the spectra were also set by the indifferent quality of the *gf*-values then available. A more detailed acknowledgement of those early studies, which nonetheless gave important qualitative insights into the nature of K-supergiant chromospheres, is given in the first paper of this series (Griffin et al., 1990, hereinafter referred to as Paper 1). The problem of contamination by the cool primary star does not occur at IUE wavelengths, where the flux contribution from a K supergiant is very small compared with that from a B dwarf. IUE spectra are therefore extremely valuable for investigating the winds and chromospheres of ζ Aur-type systems; they form the basis of the ongoing series, "A study of uv spectra of ζ Aur/VV Cep systems" in this journal (e.g. Che et al., 1983; Schröder, 1985, 1986), and their benefits are summarized by Schröder (1988).

The subtraction technique developed for handling spectra of composite stars (Griffin, 1986) now offers a powerful method for isolating the chromospheric absorption features that appear at optical wavelengths during an atmospheric eclipse. Studies of optical spectra complement those based on IUE observations and carry certain advantages:

— The chromospheric absorption-line spectrum is less crowded in the optical uv than at IUE wavelengths, so measurements can be made on intrinsically weak lines that contain information about the lowest layers of the chromosphere, if observations are made at a deep chromospheric or partial-eclipse phase.

— More neutral atomic species are observable. n_e and T_e can then be determined empirically by appeal to well-studied ionization equilibria such as Fe II/I and Mg II/I, given good atomic data.

— The optical spectra include the Balmer series, from which important information about the physical state of hydrogen can be inferred.

— The coudé spectrograph of the 2.2-m telescope at Calar Alto (DSAZ), where the data described in Paper 1 were obtained,

Send offprint requests to: K.-P. Schröder (Hamburger Sternwarte, F.R. Germany)
⋆ Visiting Astronomer, German-Spanish Astronomical Centre, Calar Alto, operated by the Max-Planck-Institut für Astronomie, Heidelberg, jointly with the Spanish National Commission for Astronomy

offers better S/N ratios and higher resolution than are available from standard IUE observations. Equivalent widths of weaker lines can therefore be measured with greater accuracy, and the empirical curves of growth constructed from them can be extended well down into the linear, density-sensitive region. The improved accuracy of the derived column densities is then limited chiefly by the quality of the available atomic data (*gf*-values).

Chromospheric absorption features can be isolated by subtracting the spectrum of the K star (i.e. the total-eclipse spectrum) point by point from each composite chromospheric-eclipse spectrum. A discussion of the technique has been given by the Griffins (1986). The result of each subtraction is a different chromospheric absorption spectrum corresponding to a particular projected height of the line of sight to the B star; each is superposed on the spectrum of ζ Aur B, which itself exhibits a few broad lines of ionized metals, He I and the Balmer series as far as about H_{17}. Unfortunately, poor observing conditions during the observing run, which was planned for the ingress and early totality of the 1987 November/December eclipse of ζ Aur, restricted our observations to two chromospheric phases, Nov. 16.1 and Nov. 17.1 U.T. (the latter during partial eclipse) and to two nights during total eclipse.

2. Interpretation of chromospheric absorption-line spectra by the method of curves of growth

2.1. Theoretical curves of growth

From IUE-based studies of chromospheres (Schröder, 1985, 1986) we know that, as the height h from the K-star limb decreases, the scale height $\alpha(h)$ decreases to values that are much smaller than the radius of the B star. The latter cannot therefore be regarded as a point light-source for purposes of interpreting absorption lines from the lower chromospheric layers. By taking into account both the density gradient (as a free parameter) and the detailed geometry we have calculated new theoretical curves of growth. Figure 1 depicts the unobstructed part of the B star divided into strips i, each strip corresponding to an individual column density N_i and a projected height h_i (the distance to the point where the line of sight passes tangentially through the chromosphere). Each individual profile is described by a saturated Gaussian profile (pure absorption):

$$I_i = I_0 \exp(-A_i \exp(-(\Delta\lambda/\Delta\lambda_D)^2)),$$

where

$$A_i = \frac{\pi e^2}{m_e c^2} \frac{\lambda \cdot c}{v\sqrt{\pi}} gf \frac{N_i^{ion}}{Z(T)} \cdot \exp(-E_i/kT_{exc}),$$

and $Z(T)$ is the partition function at temperature T. Equivalent widths are calculated by numerical integration over the average of these profiles, the average being formed by weighting each individual profile according to the length of its strip. The new curve of growth differs materially from one calculated for a point light-source: the effects of saturation in the lower and significantly denser layers now extend down into what for a point source would be the linear part of the curve, and thereby reduce its slope. Hence an observation at a single height point that populates well the lower part of a curve of growth will by itself contain some information about the density distribution in front of the B star.

When the linear parts of theoretical curves of growth are combined with those from empirical ones we find that the saturation effects become much too pronounced if we use potential density representations like $N \sim h^{-b}$. But such a density law presupposes that scale heights $\alpha \to 0$ for heights $h \to 0$, and a much better match to the linear part is possible with column density representations that use a constant scale height (β). That result is not really surprising: although densities in the upper chromosphere are represented very well by a power law in which the scale height is nearly proportional to height (Schröder, 1985), a study of the continuous uv opacity in the lower chromosphere (Schröder, 1986) suggests that the power law representing neutral hydrogen density for modelling Rayleigh scattering has a smaller exponent, i.e. a more gentle increase as $h \to 0$, than that pertaining in the outer layers. Although the theoretical curve of growth is not very sensitive to the actual value of β, we find a reassuring correspondence between it ($\beta = 1 \ldots 2\,10^6$ km) and the scale height values derived later from most of the density models ($\sim 1.2 \ldots 2.0\,10^6$ km). Considering that we have here spectroscopic information from only two height points, we are therefore justified in modelling the density of the lower chromosphere (at $h \to 0$) simply by an exponential representation. The constant scale height thereby implied of course represents an average value of a scale height $\alpha(h)$ that is actually increasing slowly with h. It may also be mentioned that the assumption of a turbulent atmosphere in hydrostatic equilibrium ($\alpha = v_{turb}^2/2g$) would yield $\alpha = 1.5\,10^6$ km (for $M_K = 6.9\,M_\odot$, $R_K = 166\,R_\odot$ and $v_{turb} = v_{sto} = 1.4$ km s^{-1}), in good agreement with those values of α observed. However, stochastic velocities are supersonic and therefore contradict the basic supposition of this simple relationship.

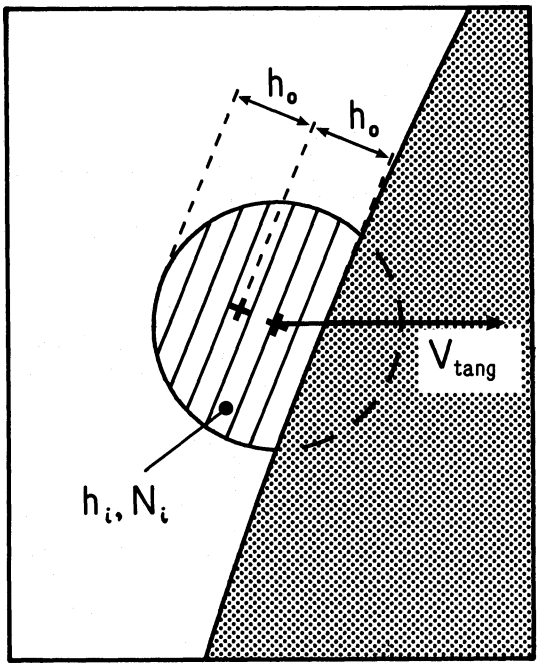

Fig. 1. Scale diagram of geometry of eclipse ingress, defining the parameter h_0 used in the text. The uneclipsed disk of the B star is treated as a series of strips i, each of which shines through a different chromospheric column density $N_i(h_i)$

2.2. Empirical curves of growth

In Paper 1 we show tracings (Fig. 5) of the chromospheric absorption-line spectrum as it appeared on 1987 Nov. 16.1

Table 1. Summary of absorption-line measurements and atomic data, ζ Aur, 1987 eclipse

(a) H I ($n=2$), $E_1=10.2$ eV. Atomic data from Wiese et al. (1966)

λ(Å)	log $gf(g=8)$	log (W_λ/λ)	
		Nov. 16.1	Nov. 17.1
3658.64	−3.1512	−4.90±0.12	−4.70 ±0.12
3659.42	−3.1120	−4.80±0.12	
3660.28	−3.0717	−4.65±0.12	
3661.22	−3.0300	−4.64±0.12	−4.22 ±0.06
3663.41	−2.9424	−4.61±0.12	−4.15 ±0.08
3664.68	−2.8962	−4.52±0.08	
3666.10	−2.8484	−4.56±0.10	−4.20:±0.08
3667.68	−2.7987	−4.47±0.07	−4.18 ±0.08
3669.47	−2.7470	−4.41±0.06	
3671.48	−2.6931	−4.35±0.07	< −4.01 ±0.08*
3673.76	−2.6369	−4.34±0.06	
3676.37	−2.5781	−4.23±0.05	−3.99 ±0.04
3679.36	−2.5165	−4.22±0.05	−4.04:±0.08
3682.81	−2.4518	−4.17±0.04	< −3.82 ±0.04*
3686.83	−2.3837	−4.15±0.04	
3691.56	−2.3117	−4.10±0.03	−4.14 ±0.06
3697.15	−2.2354	−4.03±0.03	< −3.96 ±0.06*
3703.86	−2.1542	−4.04±0.03	

Note: lines marked (*) are blends and the measurement represents an upper limit for the contribution of H I.

Table 1 (continued)

(b) Ti II. Atomic data from Wiese and Fuhr (1975). $Z(T_{exc}=5000\,K)=53.5$

λ(Å)	E_1(eV)	log gf	log (W_λ/λ)	
			Nov. 16.1	Nov. 17.1
3685.19	0.607	+0.20	−3.71±0.02	−3.65±0.02
3706.22	1.566	−0.60	−4.38±0.04	
3741.63	1.582	−0.14	−4.17±0.02	−3.94±0.04
3757.68	1.566	−0.49	−4.37±0.04	
3759.29	0.607	+0.22	−3.70±0.02	−3.68±0.02
3761.32	0.573	+0.12	−3.72±0.02	−3.70±0.04
3776.06	1.582	−1.37	−5.07±0.12	
3786.33	0.607	−2.00	−4.95±0.2	
3813.39	0.607	−1.99	−4.54±0.04	−4.02±0.06
3814.58	0.573	−1.69	−4.34±0.04	−3.95±0.02
3882.28	1.116	−1.71	−4.99±0.15	−4.15±0.1
3900.55	1.130	−0.45	−3.97±0.02	−3.74±0.05
3913.46	1.116	−0.53	−4.02±0.02	−3.85±0.04
3932.01	1.130	−1.78	−4.71±0.08	
4287.89	1.080	−2.01	−4.86±0.08	−4.09±0.04
4290.22	1.165	−1.10	−4.27±0.02	
4300.05	1.180	−0.75	−4.06±0.02	
4312.86	1.165	−1.31	−4.37±0.02	−4.06±0.04
4314.98	1.161	−1.41	−4.44±0.03	−3.85±0.06
4337.92	1.080	−1.12	−4.23±0.04	
4344.29	1.084	−2.08	−4.89±0.12	−3.95±0.06
4394.06	1.221	−1.87	−4.95±0.12	−4.29±0.06
4399.77	1.237	−1.45	−4.48±0.05	−4.14±0.04
4417.72	1.165	−1.42	−4.45±0.04	−4.13±0.06
4443.80	1.080	−0.81	−4.07±0.02	
4450.49	1.084	−1.59	−4.53±0.04	
4464.46	1.161	−2.07	−5.03±0.12	−4.06±0.06
4468.49	1.130	−0.77	−4.02±0.02	−3.96±0.04
4501.27	1.116	−0.86	−4.10±0.02	−4.07±0.04
4533.97	1.237	−0.76	−4.15±0.03	−4.08±0.04
4563.76	1.221	−0.95	−4.23±0.04	−4.13±0.04
4571.97	1.572	−0.53	−4.16±0.03	−3.97±0.04

shortly before first contact of the eclipse, and include a list of some 260 identified features. That paper comments on the need for, and our efforts to obtain, high S/N ratios: in a subtraction procedure the signal is subtracted but the noise is added. The resulting chromospheric spectra, from which we have measured equivalent widths for analysis in the present paper, therefore show unavoidably poorer S/N ratios than do the original data, and not all of the identified lines can be considered of sufficient quality for inclusion here. The number of useable lines available to us has also been restricted by the following considerations:

— The lines must be unblended. As the line of sight to the B star passes through successively deeper chromospheric layers they give rise to an increasingly rich absorption-line spectrum, although the blending remains much less severe than at IUE wavelengths.

— The strengths of the lines have to lie within useful limits, strong enough to offer accurate measurement but not so strongly saturated as to lose the density information.

— The lines should be members of low-excitation multiplets having accurate *gf*-values, if their equivalent widths are to be converted accurately into total column densities.

From the original list we selected a total of 97 lines, of H I (Balmer series), Mg I, Ti II, Fe I and Ba II, which satisfy the above criteria; they are given in Table 1 together with excitation potentials, log *gf* values and the equivalent widths measured at the two observed chromospheric phases. In the case of the Balmer lines, it was important to distinguish between the chromospheric contributions and the profiles intrinsic to the pure B star; that was achieved by reference to the out-of-eclipse spectrum of ζ Aur B which is illustrated in Fig. 4a of Paper 1, where its derivation is also described.

Separate analyses of the 0.6, 1.1 and 1.6 eV lines of Ti II yielded an excitation temperature T_{exc} of 5300±500 K at both phases. The Fe I lines at 0.0, 0.9 and 1.5 eV also gave $T_{exc}\simeq 5000$ K, though with more uncertainty, and since the combined curve of growth is not seriously sensitive to the actual value of an excitation temperature of that order we finally adopted a value of 5000 K and used it throughout when converting equivalent widths of Ti II, Fe I and Mg I into their respective total column densities. Because Ti II is the dominant ionization stage of that element at the relevant heights in the chromosphere, its density can be equated with the total density of titanium. The dominant ionization states of iron, magnesium and hydrogen are Fe II, Mg II and H I; neither of those ions nor the ground-state level of H I can be observed directly in our spectra, so solar relative abundances, as reviewed by Aller (1987), have been invoked to infer from Ti II densities the Fe II, Mg II and H I total densities.

Table 1 (continued)
(c) Fe I. Atomic data from Banfield and Huber (1973) (A), Blackwell et al. (1979a, b) (B), Corliss and Bozman (1962) (C). $Z(T_{exc}=5000\,K)=27.0$

λ(Å)	E_l(eV)	log gf	Ref.	log (W_λ/λ)	
				Nov. 16.1	Nov. 17.1
3687.47	0.86	−0.78	A	−4.52±0.04	
3705.57	0.05	−1.33	A	−4.31±0.03	
3709.25	0.91	−0.57	A	−4.37±0.04	−3.91±0.06
3719.95	0.00	−0.45	A	−3.99±0.02	
3722.56	0.09	−1.28	A	−4.34±0.04	
3733.32	0.11	−1.41	A	−4.48±0.06	
3737.14	0.05	−0.60	A	−4.01±0.03	
3743.36	0.99	−0.82	A	−4.56±0.04	−4.00±0.04
3748.26	0.11	−1.06	A	−4.16±0.04	
3749.49	0.91	+0.09	A	−3.98±0.04	
3758.24	0.96	−0.03	A	−4.19±0.03	−3.78±0.10
3763.79	0.99	−0.21	A	−4.23±0.04	−3.74±0.06
3767.19	1.01	−0.34	A	−4.37±0.04	
3787.88	1.01	−0.77	A	−4.63±0.06	−3.88±0.04
3795.00	0.99	−0.65	A	−4.52±0.06	−3.93±0.05
3812.96	0.95	−1.06	B	−4.74±0.10	−4.02±0.06
3815.84	1.48	+0.35	A	−4.25±0.02	−3.83±0.05
3820.43	0.86	+0.12	B	−4.04±0.02	
3824.45	0.00	−1.36	B	−4.42±0.04	−3.86±0.04
3825.88	0.91	−0.04	B	−4.12±0.03	−3.82±0.04
3834.23	0.96	−0.30	B	−4.36±0.04	
3840.44	0.99	−0.51	B	−4.40±0.03	
3850.00	1.01	−0.87	B	−4.63±0.06	−3.93±0.05
3856.37	0.05	−1.29	B	−4.32±0.03	−3.77±0.05
3859.91	0.00	−0.71	B	−4.10±0.02	−3.73±0.08
3865.53	1.01	−0.98	B	−4.68±0.04	−3.98±0.04
3872.50	0.99	−0.93	B	−4.58±0.04	
3878.02	0.95	−0.91	B	−4.55±0.06	
3886.28	0.05	−1.08	B	−4.25±0.04	
3887.05	0.91	−1.14	B	−4.68±0.08	
3895.56	0.11	−1.67	B	−4.65±0.06	−3.93±0.08
3899.71	0.09	−1.53	B	−4.49±0.06	−3.91±0.08
3906.45	0.11	−2.24	B	−4.86±0.12	−3.84±0.05
3920.26	0.12	−1.75	B	−4.47±0.04	−3.85±0.04
3922.91	0.05	−1.65	B	−4.51±0.04	−3.84±0.05
3930.30	0.09	−1.46	B	−4.53±0.04	
4202.03	1.48	−0.29	C	−4.70±0.04	−3.94±0.04
4250.79	1.55	−0.38	C	−4.88±0.06	−4.00±0.04
4271.76	1.48	+0.16	C	−4.42±0.04	
4325.76	1.60	+0.24	C	−4.45±0.04	
4383.55	1.48	+0.35	C	−4.19±0.03	
4404.75	1.55	+0.11	C	−4.46±0.04	
4415.12	1.56	−0.09	C	−4.81±0.08	

In Table 2 we list total ion column densities and stochastic velocities, together with the dates of observation and h_0, the projected height of the B star's centre above the limb of the supergiant. During partial eclipse, h_0 and all other parameters refer to a point mid-way between the giant's limb and the outer B-star limb (see Fig. 1). In particular, each column density as derived from a comparison with theoretical curves of growth has been defined in relation to h_0, since of course the individual strips i are observed through quite different column densities N_i. The total hydrogen column density given by Table 2 is based on the Ti II column density; its value is confirmed, with an uncertainty no greater than the uncertainties of abundances and measurements, by reference to the Sc II column density, which was derived from a few Sc II absorption lines not included in Table 1. Curves of growth for Ti II, H I and Fe I are illustrated in Fig. 2.

3. Density models

The conversion of column densities into volume densities requires some assumptions, such as spherical symmetry, about the density distributions. From analyses of high-resolution IUE spectra Schröder (1985, 1986) found the observed column densities in the middle and upper chromospheres of 31 Cyg, 32 Cyg and ζ Aur to be well fitted by power-law representations for the density. Numerical integrations along various lines of sight in the model can be compared directly with observed column densities, and such a set easily fixes the two parameters of the power law representing the density itself.

For the present work only two height points in the lower chromosphere are available. We have already pointed out that scale heights do not vary very strongly with height in the lower layers, and we felt justified in restricting the model to exponential density representations – in fact, to the familiar barometric law

$$n(h)=n_0\exp(-h/\alpha).$$

The parameters describing the geometry of the eclipse are determined in Paper 1 from our spectrophotometry combined with a critical review of previous eclipse data. All projected heights and density representations given in Tables 2–5 have been calculated according to these geometrical parameters. The density representations which are found to match best the observed column densities are summarized in Table 3 and illustrated in Fig. 3.

The height scale still includes some uncertainty that is introduced through the choice of the B-star radius, through the mass ratio (which enters via the relative mean tangential velocity, $\bar{v}_{tang}$) and through the timing of the second contact (the last affecting directly the values used to represent the distance of the centre of the B star from the limb of the K star on the two nights in question), but the impact of the error on densities is small in comparison with other uncertainties, which are typically of the order of 0.1 to 0.2 dex. On the other hand, scale heights are sensitive to the angle of ingress and may be uncertain (on an absolute scale) by about 50%.

4. Ionization equilibria, electron density and excitation

From a combination of Fe and Mg ionization equilibria we are able to determine n_e and, with less certainty, T_e from the rate equations

$$\frac{n(\text{Fe I})}{n(\text{Fe II})}=n_e\frac{\alpha(\text{Fe I},\,T_e)}{\Gamma(\text{Fe I})}\quad\text{and}\quad\frac{n(\text{Mg I})}{n(\text{Mg II})}=n_e\frac{\alpha(\text{Mg I},\,T_e)}{\Gamma(\text{Mg I})},$$

where the recombination coefficients $\alpha=\alpha_r+\alpha_d$ depend on electron temperature and photoionization rates Γ in the B-star radiation only. Collisional ionization and photoionization by the

Table 1 (continued)
(d) Ba II ($Z(T_{exc}=5000\,K)=4.2$) and Mg I ($Z(T_{exc}=5000\,K)=1.02$). Atomic data from Wiese et al. (1969) (D)

	λ(Å)	E_l(eV)	log *gf*	Ref.	log (W_λ/λ)	
					Nov. 16.1	Nov. 17.1
Ba II	4554.04	0.00	(0.0)	Adopted	−4.90±0.12	−3.95±0.04
Mg I	3838.29	2.72	0.490	D	−3.93±0.04	−3.78±0.04
Mg I	3832.30	2.71	0.270	D	−4.04±0.04	−3.81±0.08
Mg I	3829.35	2.71	0.208	D	−4.22±0.02	−3.81±0.02

Note: The uncertainties shown in Table 1 are estimated measuring errors, and do not include possible systematic errors.

Table 2. Column densities for ζ Aur, 1987 eclipse

	Nov. 16.1 U.T. $h_0=6.13\,10^6$ km	Nov. 17.1 U.T. $h_0=2.25\,10^6$ km
log *N* (H I, $n=2$)	15.65±0.10	16.0±0.2
v_{sto} (H I)	15^{+5}_{-2} km s^{-1}	15: km s^{-1}
log *N* (Mg I)	15.25±0.25	16.5±0.5
log *N* (Ti II)	16.15±0.1	17.0±0.25
v_{sto} (Ti II)	14±2 km s^{-1}	12.5±2 km s^{-1}
log *N* (Fe I)	14.80±0.15	16.15±0.2
v_{sto} (Fe I)	13±3 km s^{-1}	12.5±3 km s^{-1}
log *N* (Ba II)	12.0±0.4	13.5±0.5

Table 3. Particle densities, represented by $n(A)=n_0(A)\exp[-h/\alpha(A)]$. The last column contains the scale height of each atom or ion

A	n_0(cm^{-3})	$\alpha(A)$(10^6 km)
From observation:		
H I ($n=2$)	$2.8\,10^3$:	4.6:
Mg I	$5.2\,10^4$	1.35
Ti II	$8.0\,10^4$	2.0
Fe I	$2.8\,10^4$	1.25
From Ti II density, using solar abundances (Aller, 1987):		
H, total	$7.0\,10^{11}$	2.0
Mg II	$3.0\,10^7$	2.0
Fe II	$2.8\,10^7$	2.0

K-star radiation can both be neglected on account of the dominating presence of the hot B star. Pure photoionization from the radiation field of the B star therefore balances recombination, which depends on the local electron density and electron temperature. The ionization ratios n_I/n_{II}, given by Table 4, are obtained from the density models (see Table 3). It should be pointed out here that, since scale heights are not the same for neutral as for ionized metals, the ionization ratios are not equal to (although they are not very different from) corresponding column-density ratios. The quoted uncertainties include both observational errors and those introduced through excitation terms, especially for Mg I.

Photoionization rates Γ were calculated with the help of Kurucz (1979) model fluxes for $T_{eff}=15{,}000$ K (from Erhorn, 1990), $R_B=3.5\,10^6$ km, at a distance $r_B=5.0\,10^8$ km from the relevant (most dense) chromospheric layers in the line of sight, and a continuous opacity $\tau_c=0.17$ at the lower height point:

$$\Gamma=\int_{912\text{Å}}^{\lambda_0}\frac{4\pi}{hc}J_\lambda\lambda a_\lambda d\lambda=\frac{W4\pi}{hc}\int_{912\text{Å}}^{\lambda_0}F_{*\lambda}\lambda a_\lambda d\lambda,$$

where $W=(R_B/2r_B)^2\exp(-\tau_c)$ is a dilution factor. τ_c is a combination of Rayleigh scattering and line absorption. $\lambda_0=1576$ Å for Fe I and 1622 Å for Mg I.

Photoionization cross-sections a_λ for Fe I were derived by taking the relative values from Hansen et al. (1977) together with the absolute calibration given by Lombardi et al. (1978); those for Mg I were taken from Mendoza and Zeippen (1987). Recombination coefficients have been calculated by Woods et al. (1981) for Fe I and by Nussbaumer and Storey (1986) for Mg I (dielectronic values) and by Shull and van Steenberg (1982) (radiative values). The values we have used are all included in Table 4.

Before we can derive the electron density we have to know the electron temperature in order to calculate recombination coefficients. In the chromosphere of ζ Aur the electron temperature is unfortunately somewhat ill-determined because its value is such that both α(Mg I) and α(Fe I) are near minima and so do not vary as strongly as they would in other temperature regimes. However, the recombination coefficients and the electron density can be derived more accurately. If the two ionization equations are divided by one another, we obtain from the observed ionization ratios an empirical quantity $X_\alpha=\alpha(\text{Fe I}, T_e)/\alpha(\text{Mg I}, T_e)$ whose value is approximately equal to 0.59 at height $2.3\,10^6$ km, and to $0.46^{+0.4}_{-0.25}$ at $6.1\,10^6$ km. As Table 4b demonstrates, on the other hand, the atomic data yield a minimum in X_α of 0.71 at about $T_e=5500$ K. The overall result then, for both height points, is approximately $T_e=5500^{+1000}_{-2000}$ K. On the other hand, the accuracy of the value for α(Mg I, T_e) is still better than a factor of 1.2 and that for α(Fe I, T_e) is better than a factor of 2. The individual ionization equilibria together with the recombination coefficients in Table 4b, middle column, yield electron densities which are summarized in Table 5. The result, that $n_e=1.8$ to 5.0% of n_H in the observed range of heights, confirms absolutely that the lower chromosphere is almost neutral. This is easily consistent with the

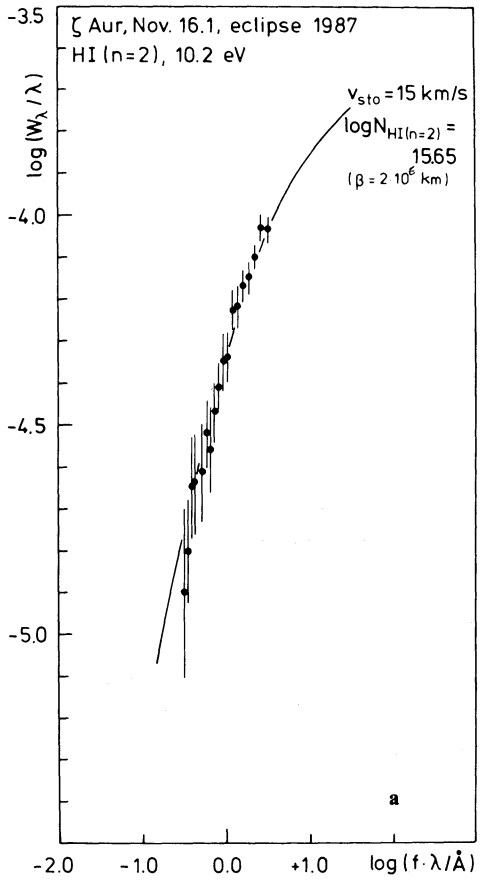

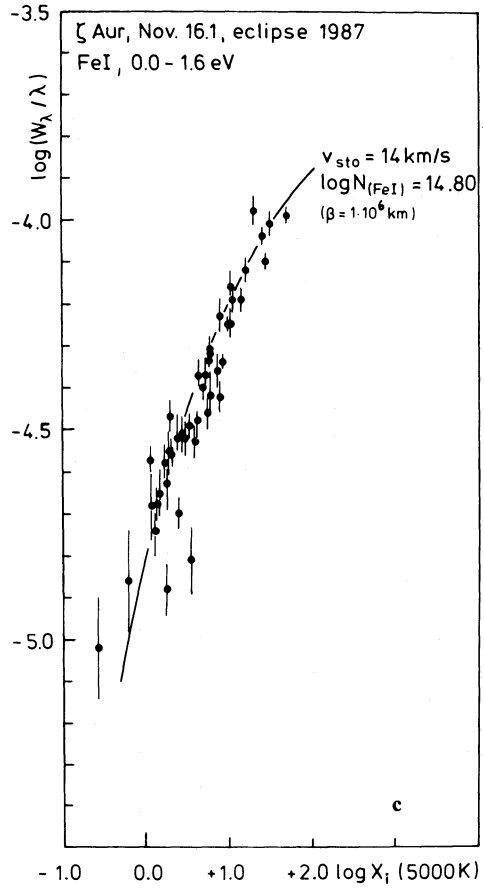

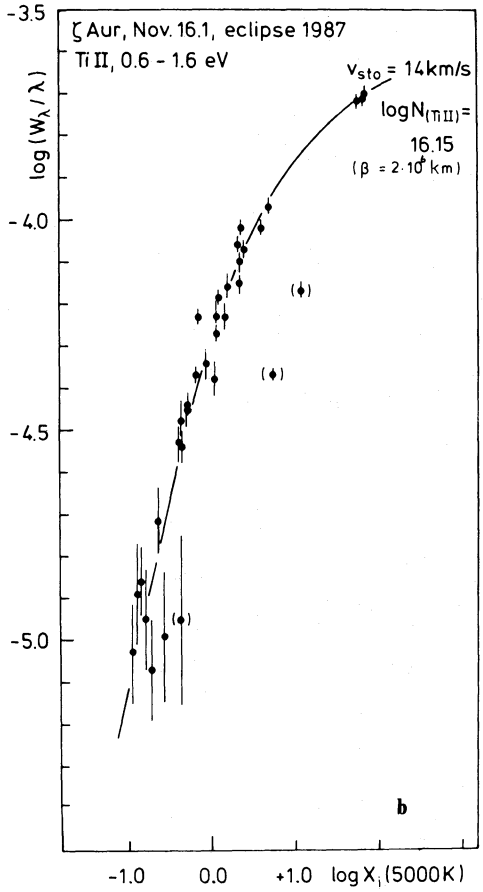

Fig. 2a–c. Curves of growth for chromospheric lines of **a** H I ($n=2$), **b** Ti II and **c** Fe I seen in the atmospheric-eclipse spectrum of ζ Aur on 1987 Nov. 16.1. $X_i = gf\lambda \exp(-E_i/kT_{exc})/Z(T_{exc})$ has been used for Fe I and Ti II. Solid lines indicate the theoretical curves of growth described in Sect. 2.1. Error bars indicate the uncertainties of the individual measurements of equivalent widths; a large contribution to the scatter may come from gf-values

observation (Schröder, 1986) that Rayleigh scattering dominates the opacity and that neutral hydrogen densities derived from it are close to the total densities. On the other hand, it is now clear that hydrogen contributes two orders of magnitude more towards the electron density than all the ionized elements put together. n_e is therefore governed by hydrogen ionization, and that information must constitute an important datum for any hydrogen model of this chromosphere. In particular, the scale heights of n_e and n_H ($n=2$) are equal – see Tables 3 and 5 and Fig. 3. It is possible that hydrogen ionization may be coupled to the mechanisms of the wind acceleration.

An excitation temperature for H I ($n=2$) can be determined quite accurately from the Balmer lines together with total neutral hydrogen densities estimated from Ti II densities (Table 3):

$$T_{exc} = \frac{-10.2\,\mathrm{eV}}{k}\left[\ln\left\{\frac{(g\,n(\mathrm{H\,I},\,n=2))}{Z(T)\,n(\mathrm{H\,I})}\right\}\right]^{-1}.$$

With $g/Z(T)=0.25$, we obtain $T_{exc}=6230\pm100$ K at height $6.1\,10^6$ km, and 5900 ± 200 K at $2.3\,10^6$ km. (For H I($n=2$)/H I, see Table 4a.) However, our values of T_{exc} are clearly greater than the excitation temperature of 5300 K for Ti II (0.6–1.6 eV), and

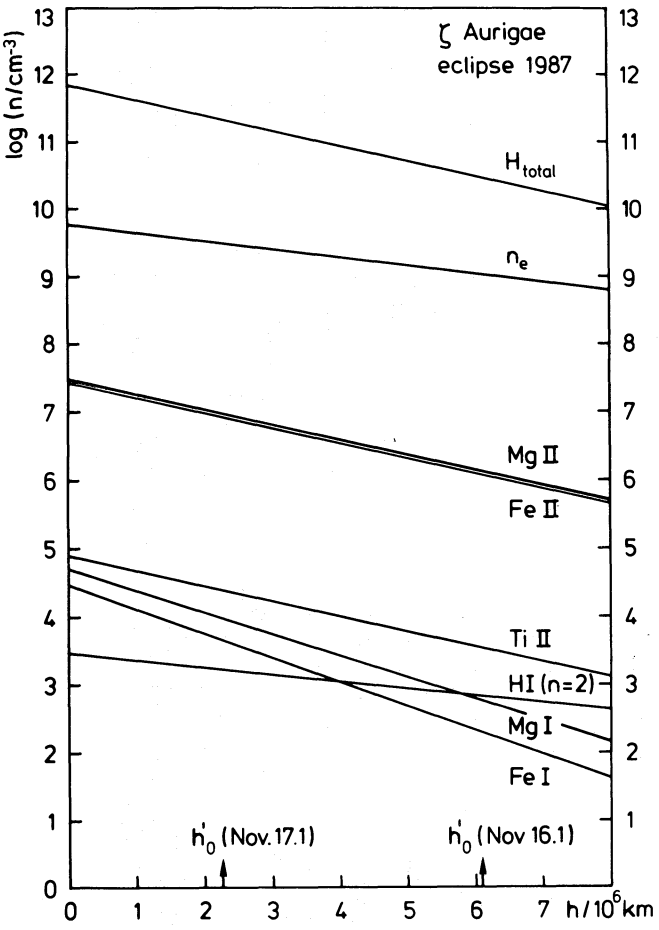

Fig. 3. Plot of the empirical densities in the lower chromosphere of ζ Aur at the 1987 eclipse ingress. The obvious differences between the density gradients of metals, ions and excited hydrogen are attributable to NLTE effects, as described in Sect. 4

serve to remind us that we are dealing here with NLTE processes in which the relative impact of the hot radiation from the companion upon the level population increases with height and with excitation energy. With increasing height, density and collision rates decrease, and larger energy differences (such as occur in the hydrogen term scheme) are lessening collision rates even more, whilst photoionization rates remain high.

It is the presence of energetic photons that is responsible for the very high degree (99.9%) of single ionization in metals such as Mg, Si, Ti, V and Fe. Another example which illustrates neatly the impact of the radiation from the companion upon metal ionization involves Ba II. Berium has a second ionization potential of 10.5 eV; that is below the Lyman limit but is well within the range of the Lα wings, where photons that are capable of ionizing Ba II experience very strong opacity from Rayleigh scattering. Our tracings show that the Ba II ground-state chromospheric absorption line, λ 4554 Å, increases much more strongly towards the lower projected height than do chromospheric lines of Ti II and Fe II, for example. It can be estimated (though the *gf*-value is rather uncertain) that about 50% of Ba exists as Ba II at $h = 2.3\,10^6$ km but only about 13% at $6.1\,10^6$ km. All lower-ionized species are favoured by increased recombination rates (owing to greater electron densities) at lower heights, and that is indeed observed for Fe I and Mg I. However, there is an additional effect in the case of Ba II: that ion is exposed to ionizing photons in the upper chromosphere only, because it is shielded well from them at lower heights by Rayleigh scattering opacity. We observe a similar effect in Y II lines, for which the same arguments apply.

5. Discussion

It was shown in the previous section that NLTE processes in the chromosphere of the K supergiant are dominated by the radiation field of the hot B-star companion. While the hydrogen excitation temperature (about 5900 to 6200 K, increasing with height) is higher than the electron temperature (some 5500 K), the excitation temperature of 5300 K for Ti II is very close to it. We may say that Ti II is in a pseudo-LTE state; Baade's (1986) discussion of Fe II similarly found evidence that a kind of UV radiative pumping mechanism in ζ Aur systems retains level populations in LTE at much lower densities than would be expected from collisional rates alone. For these reasons, our use of approximately this same excitation temperature, viz. 5000 K throughout, for deriving total densities from absorption lines of different excitation potentials is not unreasonable and does not increase the uncertainties beyond those arising from other sources.

However, the situation for hydrogen is very complex. It requires the calculation of a two-dimensional model with a cool internal radiation source and a diluted hot external one. The hot radiation is responsible for an enhanced population (increasing with height) of the excited levels ($n = 2, 3 \ldots$), which are at 75% and more of the energy required for ionization; the cool radiation of the giant (in the Balmer and Paschen continua) and collisions are then capable of ionizing only a small fraction of hydrogen via the excited levels. This process requires the scale heights of electron density and excited hydrogen to be equal, as indeed is shown in Table 3; it is also more efficient at greater heights, which explains why the scale heights of electron density and excited hydrogen are significantly larger than the scale heights of the total densities – see Fig. 3.

Since IUE and optical spectra provide accurate knowledge concerning not only the radiation fields, but also the electron density and the excitation temperature of the $n = 2$ level, a hydrogen model ought to be well-constrained by observation and should furnish us with a detailed and self-consistent picture of the chromosphere; it may perhaps give some hints as to the actual wind acceleration mechanism. The construction of a hydrogen model is to be the subject of a future paper.

All our knowledge so far on this subject is purely empirical and has been derived only from ionization equilibria for Fe and Mg. From high-resolution IUE spectra taken during the 1979 eclipse, Schröder (1985, 1986) has already attempted to determine total densities and upper limits of the electron density. Since IUE covers a different height range, a direct comparison is difficult, and there seem to be variations between different eclipses to contend with as well. Nevertheless, because those IUE data refer to greater chromospheric heights they form an interesting complement to the optical observations. Unlike the lower chromospheric layers, the upper layers show a rapidly increasing scale height, one that is nearly proportional to height. The density there is coupled to the wind acceleration by the equation of continuity, and that brings about a gentle transition into the

Table 4

(a) Observed ionization ratios, hydrogen excitation, and photoionization rates

	$h=2.3\,10^6$ km	$h=6.1\,10^6$ km
$\log \frac{n(\text{Mg I})}{N(\text{Mg II})}$	-3.00 ± 0.35	-3.40 ± 0.3
$\log \frac{n(\text{Fe I})}{N(\text{Fe II})}$	-3.3 ± 0.2	-3.80 ± 0.1
$\log \frac{n(\text{H I}, n=2)}{n(\text{H, total})}$	-8.11 ± 0.2	-7.65 ± 0.1
Γ(Fe I)	$2.2\ s^{-1}$	$2.6\ s^{-1}$
Γ(Mg I)	$1.8\ s^{-1}$	$2.2\ s^{-1}$

(b) Total recombination coefficients ($10^{-12}\,cm^3\,s^{-1}$)

	T_e(K)=3000	4000	5000	5500	6000	7000	8000
α(Mg I, T_e)	0.435	0.393	0.405	0.430	0.460	0.545	0.690
α(Fe I, T_e)	0.415	0.325	0.290	0.305	0.380	0.715	1.410
$X_\alpha=\alpha$(Fe)/α(Mg)	0.954	0.827	0.716	0.710	0.826	1.31	2.04

wind. The density representation based on IUE data comes close to the lower chromospheric densities (derived in the present paper) at a height of about $8\,10^6$ km, where $n_H \cong 2\,10^{10}\,cm^{-3}$; the precise values depend on the compatibility of the density information calculated from two different eclipses and on the slight modification to the eclipse geometry.

When we compare the electron densities in the upper and lower chromosphere, we have to point out that in this paper we have used a more reliable (experimental) photoionization cross-section which yields ionization rates Γ about a factor of 6 greater. When we apply those rates to the 1979 IUE data, the upper limits for n_e also become higher by this factor: about $7\,10^8\,cm^{-3}$ at height $8\,10^6$ km, and $1.5\,10^9\,cm^{-3}$ at $1.6\,10^7$ km, or less than about 5% and 100% degree of ionization of hydrogen, respectively. But there is no more information about the electron density itself from those IUE data, since without Mg I observations it is impossible even to guess the electron temperature. The recombination rate α(Fe I, T_e) increases strongly, by about a factor of 5, when the temperature rises from 5500 K to only about 8000 K, and that reduces the actual electron density below the upper limits (which refer to $T=5500$ K) by about the same factor. At greater heights the electron temperature should for these reasons increase from 5500 K, since the wind and the upper chromosphere are still substantially neutral, but on the other hand the IUE upper limit of n_e (100% n_H) implies that contradicting ionization degree of 100% for $T_e=5500$ K. The upper limits further suggest that, at least up to a height of about $8\,10^6$ km, the electron density may slowly decrease while the degree of ionization increases. Again, a self-consistent hydrogen model, constrained by the optical observations of the lower chromosphere and extended into the upper chromosphere, will tell us more.

Table 5. Electron density from Fe and Mg ionization equilibria ($T_e=5500$ K)

	Fe only	Mg only	Mean
$\log n_e(h_1=2.3\,10^6$ km)	9.55 ± 0.4	9.63 ± 0.4	9.59 ± 0.3
$\log n$(H, total, h_1)			11.34 ± 0.2
$\log n_e(h_2=6.1\,10^6$ km)	9.12 ± 0.3	9.31 ± 0.3	9.21 ± 0.2
$\log n$(H, total, h_2)			10.05 ± 0.1
n_e/n_H (h_1)	1.7%	1.9%	1.8%
n_e/n_H (h_2)	4.0%	6.2%	5.0%
$\alpha(n_e,\ h_1<h<h_2)$			$4.4\,10^6$ km
$n_e(h=0)$			$6.6\,10^9\,cm^{-3}$

It is now possible in principle to model other ζ Aur supergiants by these techniques. Of particular interest are the positions of the stars in the HR diagram, where giants and supergiants appear to be segregated according to the existence of either a hot corona or a cool wind (Linsky and Haisch, 1979). Fortunately some ζ Aur giants (22 Vul, HR 6902 and τ Per) lie very near to the dividing line that separates the different types, so a comparison of the chromospheric properties of those stars will be very valuable in helping us to elucidate the nature of the dividing line.

Acknowledgements. We are particularly grateful to the Max-Planck Institut für Astronomie, Heidelberg, for allocating observing time on the 2.2-m telescope at Calar Alto, and to the staff of that Observatory for help and support. We would also like to record our gratitude to Dr. P. Storey in London and to several

colleagues in Hamburg with whom we have had fruitful discussions; to the S.E.R.C., the D.F.G. and N.A.T.O. for travel and subsistence funds, and to the Leverhulme Trust for financial support for R.E.M.G.

References

Aller, L.A.: 1987, in *Spectroscopy of Astrophysical Plasmas*, eds. A. Dalgarno, D. Layzer, Cambridge University Press, Cambridge, p. 102
Baade, R.: 1986, *Astron. Astrophys.* **154**, 145
Banfield, F.P., Huber, M.C.E.: 1973, *Astrophys. J.* **186**, 335
Blackwell, D.E., Ibbetson, P.A., Petford, A.D., Shallis, M.J.: 1979a, *Monthly Notices Roy. Astron. Soc.* **186**, 633
Blackwell, D.E., Petford, A.D., Shallis, M.J.: 1979b, *Monthly Notices Roy. Astron. Soc.* **186**, 657
Che, A., Hempe, K., Reimers, D.: 1983, *Astron. Astrophys.* **126**, 225
Corliss, C.H., Bozman, W.R.: 1962, *Nat. Bur. Stand. Monogr.* No. 53
Erhorn, G.: 1989, Dissertation, University of Hamburg
Griffin, R. & R.: 1986, *J. Astrophys. Astron.* **7**, 195
Griffin, R.E.M., Griffin, R.F., Schröder, K.-P., Reimers, D.: 1990, *Astron. Astrophys.* **234**, 284 (Paper 1)
Hansen, J.E., Ziegenbein, B., Lincke, R., Kelly, H.P.: 1977, J. Phys. B **10**, 37
Kurucz, R.L.: 1979, *Astrophys. J. Suppl.* **40**, 1
Linsky, J.L., Haisch, B.M.: 1979, *Astrophys. J.* **229**, L27
Lombardi, G.G., Smith, P.L., Parkinson, W.H.: 1978, *Phys. Rev. A* **18**, 2131
Mendoza, C., Zeippen, C.J.: 1987, *Astron. Astrophys.* **179**, 346
Nussbaumer, H., Storey, P.J.: 1986, *Astron. Astrophys. Suppl.* **64**, 545
Schröder, K.-P.: 1985, *Astron. Astrophys.* **147**, 103
Schröder, K.-P.: 1986, *Astron. Astrophys.* **170**, 70
Schröder, K.-P.: 1988, in *The Symbiotic Phenomenon*, J. Mikdajewska (ed.), Kluwer, Dordrecht, p. 339
Shull, J.M., van Steenberg, M.: 1982, *Astrophys. J. Suppl.* **48**, 95
Wiese, W.L., Fuhr, J.R.: 1975, *J. Phys. Chem. Refer. Data* **4**, 263
Wiese, W.L., Smith, M.W., Glennon, B.M.: 1966, *Atomic Transition Probabilities*, 1, NSRDS-NBS 4, U.S. Govt. Printing Office, Washington
Wiese, W.L., Smith, M.W., Miles, B.M.: 1969, *Atomic Transition Probabilities*, 2, NSRDS-NBS 22, U.S. Govt. Printing Office, Washington
Wilson, O.C.: 1960, in *Stellar Atmospheres*, ed. J.L. Greenstein, The University of Chicago Press, Chicago, p. 436
Woods, D.T., Shull, J.M., Sarazin, C.L.: 1981, *Astrophys. J.* **249**, 399